

SUPPLEMENTARY MATERIALS

Single-ion magnet behaviour in mononuclear and two-dimensional dicyanamide-containing cobalt(II) complexes[†]

Anna Świtlicka-Olszewska^{*a}, Joanna Palion-Gazda^a, Tomasz Klemens^a, Barbara Machura^a, Julia Vallejo^b, Joan Cano^{b,c}, Francesc Lloret^b, Miguel Julve^{*b}

^a Department of Crystallography, Institute of Chemistry, University of Silesia, 9th Szkolna St., 40–006 Katowice, Poland, E-mail:anna.switlicka@gmail.com

^b Department of Química Inorgànica/Instituto de Ciencia Molecular (ICMol), Facultat de Química de la Universitat de València, C/ Catedrtico José Beltrán 2, 46980 Paterna, València, Spain. E-mail: miguel.julve@uv.es

^cFundació General de la Universitat de València (FGUV), Universitat de València, 96480 Paterna, València, Spain

Table S1. Short intra- and intermolecular contacts detected in the crystal structures of **1–4**.

D—H \cdots A	D—H	H \cdots A	D \cdots A [Å]	D—H \cdots A [°]
Compound 1				
C(13)—H(13) \cdots N(97l)	0.93	2.61	3.419(4)	145.4
C(14)—H(14A) \cdots N(97m)	0.97	2.62	3.495(6)	150.1
Compound 2				
C(2)—H(2) \cdots N(98n)	0.93	2.51	3.407(6)	163.7
Compound 3				
C(15)—H(15C) \cdots N(94)	0.96	2.55	3.291(6)	133.9
Compound 4				
N(4)—H(4A) \cdots N(2o)	0.86	2.35	3.209(3)	174.3
N(4)—(H4B) \cdots N(97m)	0.86	2.25	3.083(3)	163.9

Symmetry transformations used to generate equivalent atoms: (l): x,1+y,z; (m):-1/2+x,1/2-y, -1/2+z; (n): -x,1-y,1-z; (o): 1/2-x,1/2-y,1-z.

Table S2. Selected *ac* magnetic data for **1**, **2**, and **3** at different *dc* applied fields.

Compound	<i>H</i> ^a (G)	τ_0 ^b × 10 ⁶ (s)	<i>E_a</i> ^b (cm ⁻¹)	α ^c	χ_s ^c (cm ³ mol ⁻¹)	χ_t ^c (cm ³ mol ⁻¹)
1	1000	1.37	5.60	0.233 (2.5 K)	0.329 (2.5 K)	1.044 (2.5 K)
				0.227 (3.0 K)	0.281 (3.0 K)	0.898 (3.0 K)
				0.189 (3.5 K)	0.255 (3.5 K)	0.775 (3.5 K)
1	2500	0.87	7.74	0.203 (2.5 K)	0.088 (2.5 K)	0.837 (2.5 K)
				0.188 (3.0 K)	0.075 (3.0 K)	0.808 (3.0 K)
				0.160 (3.5 K)	0.070 (3.5 K)	0.739 (3.5 K)
2	500	1.44	4.53	—	—	—
2	1000	1.54	5.33	0.115 (2.6 K)	0.202 (2.6 K)	0.649 (2.6 K)
				0.095 (3.0 K)	0.182 (3.0 K)	0.577 (3.0 K)
				0.066 (3.4 K)	0.172 (3.4 K)	0.515 (3.4 K)
2	2500	0.37	9.24	0.103 (2.6 K)	0.052 (2.6 K)	0.509 (2.6 K)
				0.087 (3.0 K)	0.048 (3.0 K)	0.505 (3.0 K)
				0.069 (3.4 K)	0.047 (3.4 K)	0.478 (3.4 K)
3	500	0.72	11.48	0.099 (5.5 K)	0.288 (5.5 K)	0.299 (5.5 K)
				0.087 (6.0 K)	0.266 (6.0 K)	0.275 (6.0 K)
				0.076 (6.5 K)	0.250 (6.5 K)	0.258 (6.5 K)
3	1000	0.63	13.81	0.047 (5.5 K)	0.268 (5.5 K)	0.302 (5.5 K)
				0.042 (6.0 K)	0.255 (6.0 K)	0.286 (6.0 K)
				0.056 (6.5 K)	0.241 (6.5 K)	0.267 (6.5 K)
3	2500	0.71	15.44	0.158 (5.5 K)	0.260 (5.5 K)	0.293 (5.5 K)
				0.060 (6.0 K)	0.240 (6.0 K)	0.285 (6.0 K)
				0.021 (6.5 K)	0.227 (6.5 K)	0.269 (6.5 K)

^a Applied dc magnetic field. ^b The values of the pre-exponential factor (τ_0) and activation energy (E_a) are calculated through the Arrhenius law [$\tau = \tau_0 \exp(E_a/k_B T)$]. ^c The values of the α parameter, adiabatic (χ_s) and isothermal (χ_t) susceptibilities are calculated from the experimental data at different temperatures through the generalized Debye law (see text).

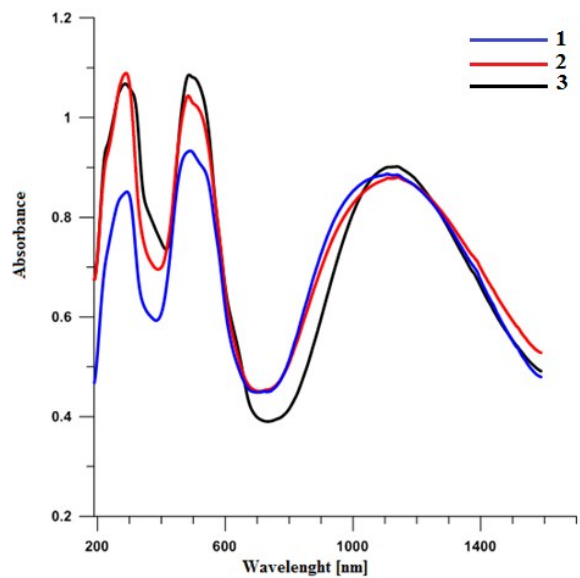


Figure S1. Solid reflectance spectra of **1–3**.

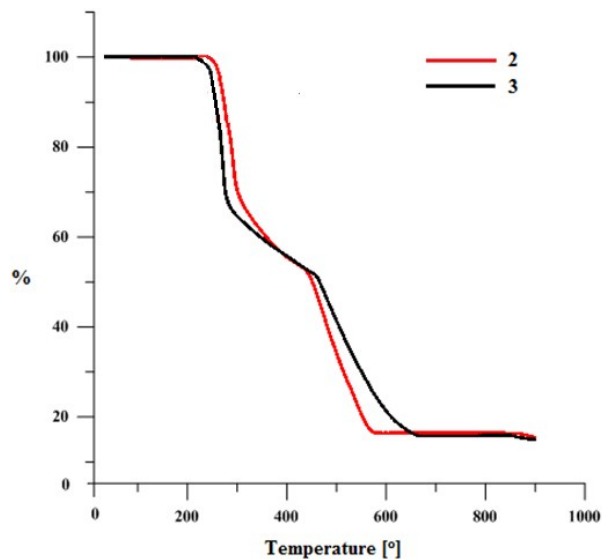


Figure S2. TGA of **2** (red line) and **3**(black line) under dry N_2 atmosphere.

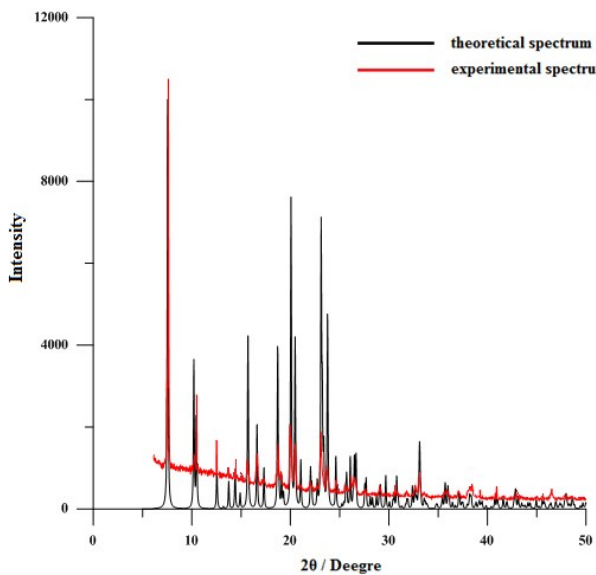


Figure S3. X–ray powder diffraction pattern of **1** at room temperature, together with the calculated pattern from the single crystal data.

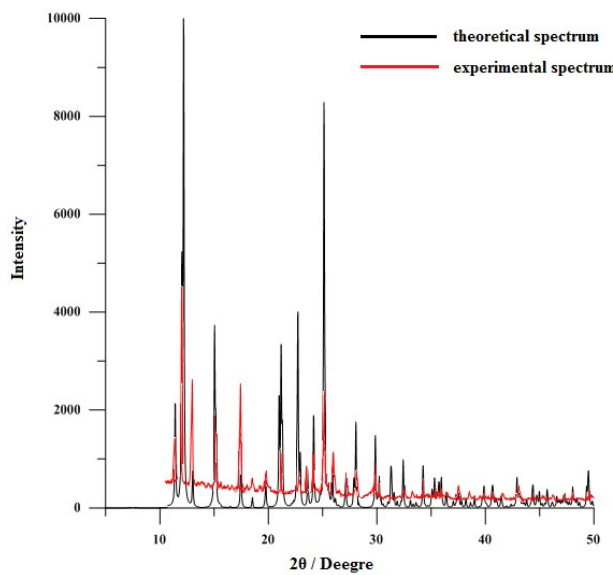


Figure S4. X–ray powder diffraction pattern of **2** at room temperature, together with the calculated pattern from the single crystal data.

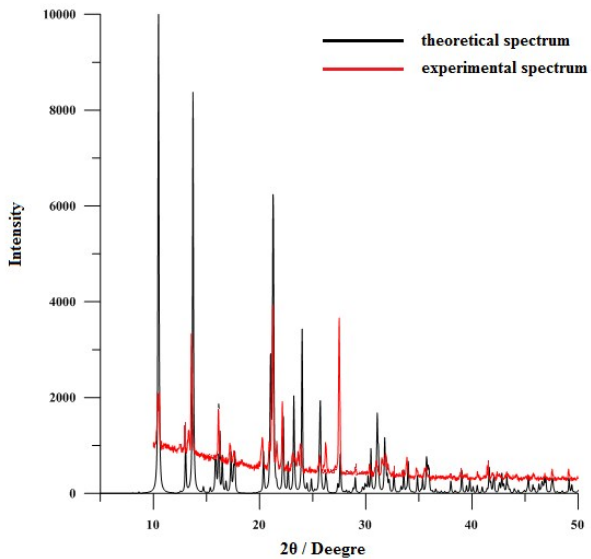


Figure S5. X–ray powder diffraction pattern of **3** at room temperature, together with the calculated pattern from the single crystal data.

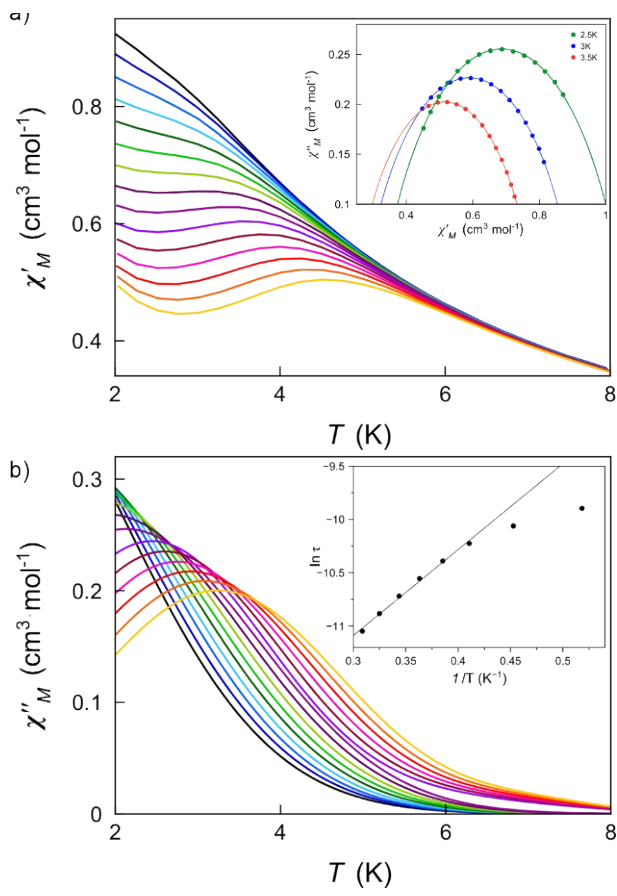


Figure S6. Frequency dependence of the in–phase (a) and out–of–phase (b) ac susceptibilities for **1** under an applied static field $H_{dc} = 1000$ G with a ± 5.0 G oscillating field at frequencies in the range 1–10 kHz. The insets show the Cole–Cole plots at 2.5, 3.0 and 3.5 K (a) and the Arrhenius plot (b) in the high temperature region. The solid lines are the best fit curves (see Table S2).

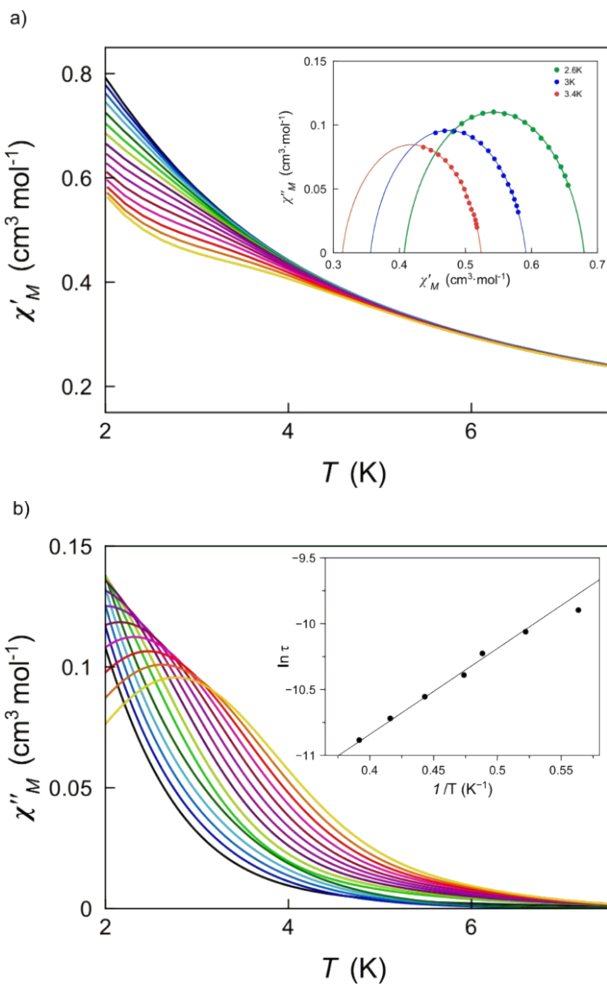


Figure S7. Frequency dependence of the in-phase (a) and out-of-phase (b) ac susceptibilities for **2** under an applied static field $H_{dc} = 500$ G with a ± 5.0 G oscillating field at frequencies in the range 1–10 kHz. The insets show the Cole–Cole plots at 2.5, 3.0 and 3.5 K (a) and the Arrhenius plot (b) in the high temperature region. The solid lines are the best fit curves (see Table S2).

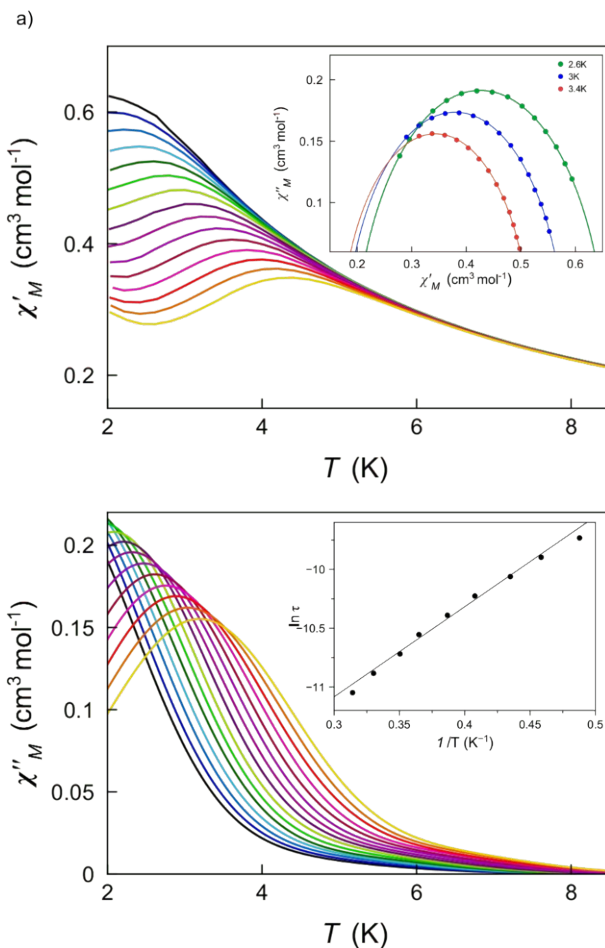


Figure S8. Frequency dependence of the in-phase (a) and out-of-phase (b) ac susceptibilities for **2** under an applied static field $H_{\text{dc}} = 1000$ G with a ± 5.0 G oscillating field at frequencies in the range 1–10 kHz. The insets show the Cole–Cole plots at 2.4, 3.0 and 3.6 K (a) and the Arrhenius plot (b) in the high temperature region. The solid lines are the best fit curves (see Table S2).

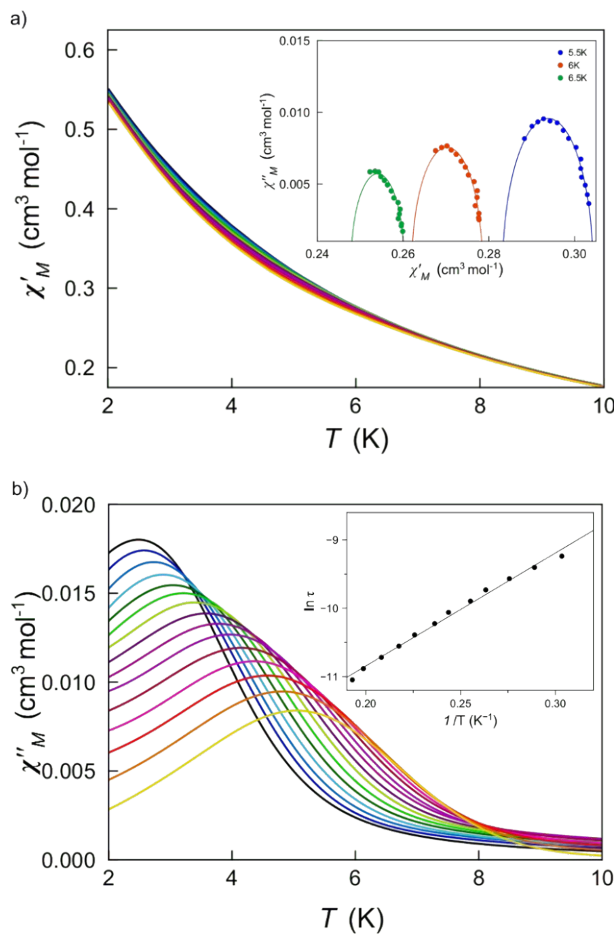


Figure S9. Frequency dependence of the in-phase (a) and out-of-phase (b) ac susceptibilities for **3** under an applied static field $H_{dc} = 500$ G with a ± 5.0 G oscillating field at frequencies in the range 1–10 kHz. The insets show the Cole–Cole plots at 5.5, 6.0 and 6.5 K (a) and the Arrhenius plot (b) in the high temperature region. The solid lines are the best fit curves (see Table S2).

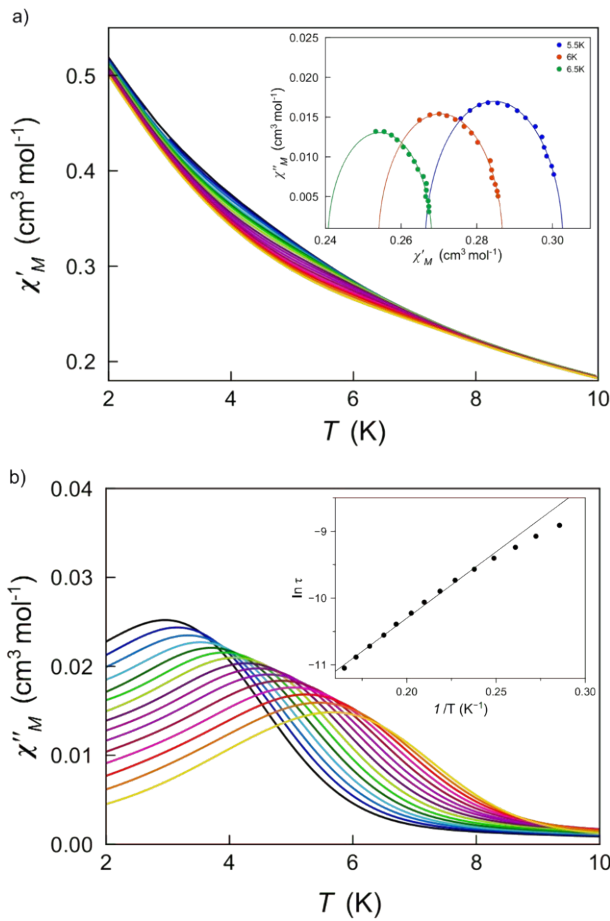


Figure S10. Frequency dependence of the in-phase (a) and out-of-phase (b) ac susceptibilities for **3** under an applied static field $H_{\text{dc}} = 1000$ G with a ± 5.0 G oscillating field at frequencies in the range 1–10 kHz. The insets show the Cole–Cole plots at 5.5, 6.0 and 6.5 K (a) and the Arrhenius plot (b) in the high temperature region. The solid lines are the best fit curves (see Table S2).